EUROGRAPHICS 2006 / E. Gröller and L. Szirmay-Kalos
(Guest Editors)

Volume 25 (2006), Number 3

A Predictive Light Transport Model for the Human Iris

Michael W.Y. Lam and Gladimir V.G. Baranoski

Natural Phenomena Simulation Group, School of Computer Science, University of Waterloo, Canada

Abstract

Recently, light interactions with organic matter have become the object of detailed investigations by image synthesis researchers. Besides allowing these materials to be rendered in a more intuitive manner, these efforts aim to extend the scope of computer graphics applications to areas such as applied optics and biomedical imaging. There are, however, organic materials that still lack predictive simulation solutions. Among these, the ocular tissues, especially those forming the human iris, pose the most challenging modeling problems which are often associated with data scarcity. In this paper, we describe the first biophysically-based light transport model for the human iris ever presented in the scientific literature. The proposed model algorithmically simulates the light scattering and absorption processes occurring within the iridal tissues, and computes the spectral radiometric responses of these tissues. Its design is based on the current scientific understanding of the iridal morphological and optical characteristics, and it is controlled by parameters directly related to these biophysical attributes. The accuracy and predictability of the spectral results provided by the model are evaluated through comparisons with actual measured iridal data, and its integration into rendering frameworks is illustrated through the generation of images depicting iridal chromatic variations.

Categories and Subject Descriptors (according to ACM CCS): I.3.8 [Computer Graphics]: Applications

1. Introduction

The realistic rendering of human features has always been a challenge for the computer graphics community. Since the current state of the art in rendering enable us to generate believable images of virtual humans, it is natural that we as researchers attempt to go a step further by looking for modeling solutions that can also lead to predictable images [Pur03]. Although these solutions usually require more resources and time to be developed and properly evaluated using actual measured data, they can make the image synthesis process more automatic and facilitate the reproduction of realistic results. Furthermore, a predictive modeling approach has a broad scope of scientific applications. Despite recent multidisciplinary efforts in this area, however, there are still human features for which predictive rendering solutions are either scarce or nonexistent. In this paper, we investigate one of these features, namely the human iris (Figure 1), arguably the most striking ocular structure affecting facial appearance.

Figure 1: *An iridal image rendered using the proposed model and framed by an artist's conception of the human eye.*

The human iris is a complex optical system, and its characteristic spectral signature is represented by chromatic attributes (*e.g.*, hue and saturation [WS82]) which are among the most readily discernible traits of the human phenotype [WSF*96]. These attributes are associated with the spectral

light distribution of the iridal tissues, and researchers from different fields have been studying the photobiological properties of these tissues for decades. In colorimetry, the investigations are oriented towards the measuring and classification of iridal chromatic attributes [TSC*01], and the study of their dependence on the distribution and content of iridal chromophores (pigments) [IWA97]. In computer vision, researchers use iridal chromaticity (specified by the dominant wavelength and purity of the iridal colour [WS82]) in estimations of environmental illumination [WLLK05]. In the medical field, the research efforts are focused on the relationship between iridal pigmentation and the incidence of several eye diseases such as the degeneration of ocular tissues [DDK91] and melanoma [REG97]. In biophysics and investigative ophthalmology, researchers examine the relationship between iridal chromatic attributes and phenomena such as the pupil size and pupillary light reflex [BASZ98]. It is worth noting that, although mechanical [WG70] and computational models [DP89, HRSM95, HS02, PC02, vNT86] have been proposed in the biomedical literature to investigate the processes that control the amount of light that enters the human eye, these models are aimed at the light interactions with ocular fundus tissues such as the retina. The processes of light propagation and absorption within the iridal tissues are outside the scope of these models. Incidentally, the human iris is also object of investigation in biometrics due to the uniqueness of its texture patterns (the probability of two irides agreeing is about one in seven billion [DD01]), which can be used in identification methodologies [Wil97].

In the computer graphics literature, few papers related to the human eye's appearance have been published to date. In their research aimed at ocular surgical simulations, Sagar et al. [SBM*94] used a Gouraud shaded polygon with colours specified by a colour ramp to represent the human iris. Halstead et al. [HBKM96] proposed an algorithm for the reconstruction of curved surfaces from specular reflection patterns that can be applied on the measurement of the outermost ocular tissue, namely the human cornea. Lefohn et al. [LCR*03] presented the first biologically motivated algorithm specifically designed for the rendering of realistic looking irides. Their modeling approach is based on an ocular prosthetics methodology. According to Lefohn et al. [LCR*03], the development of a biophysically-based procedural solution for the rendering of the human iris would have to overcome obstacles associated with the inherent complexity of the iridal tissues and data scarcity. Despite the fact that the biophysical processes of light interaction with these tissues have not been simulated by Lefohn et al. [LCR*03], it is important to note that their modeling approach includes the geometrical attributes of the human iris, and it can produce believable images of the human eye. Also aiming at iridal image synthesis, but using an image processing paradigm, Wecker et al. [WFG05] proposed a technique to decompose iridal images into several components. These are then recombined to generate a new image. Recently, Deering [Dee05] presented an algorithm to model ocular photoreceptor cells, and carefully examined visual perception issues. Although his work was not aimed at the rendering of the human iris, it further expanded the biophysical foundation for eye-related research in computer graphics.

In this paper, we propose a novel predictive light transport model for the human iris. Our investigation is aimed at computer graphics and tissue optics applications, and it focuses on light-matter interaction issues, *i.e.*, morphogenetic issues responsible for the distinctiveness of the iridal texture patterns are beyond the scope of this work. The proposed iridal light transport model, henceforth referred to as the ILIT model, takes into account the mechanisms of light propagation and absorption in the iridal tissues, and it is controlled by biophysically meaningful parameters.

The ILIT model is implemented using Monte Carlo techniques [Pra88], and its accuracy and predictability are evaluated through comparisons of modeled results with actual measured iridal data, as well as observations of actual phenomena reported in the scientific literature. The complete biophysical data set used in our evaluation experiments is provided so that they can be seamlessly reproduced by computer graphics and biomedical researchers. We also present images of human irides rendered using the ILIT model to illustrate its qualitative capabilities and its potential use in image synthesis pipelines.

The remainder of this paper is organized as follows. The next section provides a concise overview of the human eye, and a more detailed description of the iris with an emphasis on factors affecting the light interaction with iridal tissues. Section 3 presents the ILIT model. Section 4 outlines our evaluation approach and provides the biophysical data set used in our simulations. Section 5 presents the results of the quantitative and qualitative experiments used to evaluate the accuracy and predictability of the ILIT model, as well as iridal images obtained by integrating it into a standard rendering framework. The paper closes with a summary and directions for future work.

2. Biophysical Background

In this section, we briefly examine the visible ocular tissues, and define the biophysical terms used throughout this paper. We also present qualitative and quantitative biophysical information used in the design of the ILIT model. The reader interested in a more comprehensive description of the ocular anatomy and physiology is referred to classical books on these topics [FDML02, SL89].

2.1. Overview of Ocular Tissues

The shape of the human eyeball can be approximated by two incompletely overlapping spheres with different radii, with the smaller sphere positioned in the front of the face. Its

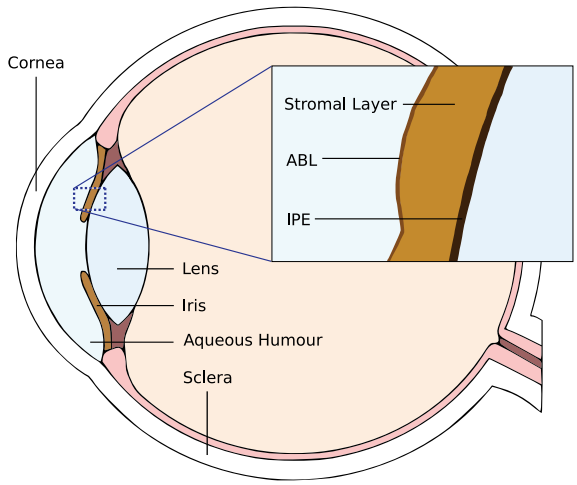

Figure 2: *Sketch showing the visible ocular tissues and a zoom in of the iridal layers.*

appearance is mostly determined by the interaction of light with five ocular media illustrated in Figure 2, namely cornea, sclera, lens, aqueous humor and iris.

The sclera contains the "white" part of the visible eyeball, and the cornea is a clear tissue, serving as its only entrance of light. In its normal state, the cornea appears transparent, and it is covered by a tear film that makes its surface optically smooth [HBKM96]. The space between the cornea and the lens, a colourless tissue, is occupied by the aqueous humor, a clear alkaline liquid. Although measurements of cornea and aqueous humor transmittance [BW62, BvB90, vdBT94] suggest a slight wavelength dependence, it is important to note that such measurements did not include backscattered light which may also affect the spectral signature of these media.

The iris is a thin pigmented diaphragm stretching across the front of the eye and surrounding the pupil. Due to the support of the neighboring lens, it has a cone-like shape pointing towards the front of the eye. It can be described as a multilayered tissue (Figure 2), and its spectral signature is determined by its morphological and optical characteristics, which are concisely described in the following section.

2.2. Iridal Morphological and Optical Characteristics

The outermost iridal layer is the ABL (Anterior Border Layer). It consists of a dense arrangement of pigmented cells, collagen fibers and fibroblasts [Eag88, SL89]. Immediately behind the ABL, we find the Stromal Layer. Although both layers consist of connective tissue and pigmented cells, the Stromal Layer is less dense than the ABL [Eag88]. The Stromal Layer is also characterized by the presence of loosely arranged collagen fibrils. The innermost layer is an opaque tissue called IPE (Iris Pigment Epithelium). It consists of heavily pigmented epithelial cells which are tightly fused by intercellular connections [IWA97].

The primary factors affecting the iridal chromatic attributes are the density and pigmentation of the iridal tissues [IWA97]. Most of the chromatic variations observed in the human iris are due to iridal pigmentation, specially that of the ABL [IWA97, Wil97]. However, as pointed out by Delori et al. [DDK91], instead of a simple continuum with pigment content, there are discrete families of spectral signatures which cannot be predicted by a simple absorption model. When there is little pigmentation in the ABL, the iridal spectra is dominated by tissue scattering [DDK91], *i.e.*, light is scattered by stromal collagen fibrils.

The scattering caused by the stromal collagen fibrils occurs in a Rayleigh fashion [WSF*96] which is proportional to the forth power of the light frequency [Str71]. Hence, it may produce grey or blue hues since shorter wavelengths are preferentially attenuated [DDK91, WSF*96, Wil97]. As light gets scattered multiple times inside the iridal layers, its spatial distribution quickly becomes diffuse. As a result, the iridal surface scattering distribution has a near-Lambertian profile [BVM02, Wil97].

Among the iridal pigments, the melanin provides the most significant qualitative and quantitative contributions to the variations in the iridal chromatic attributes, which are directly affected by the total content and distribution of this pigment in the ABL and the Stromal Layer [MWP*92, IBK*96]. The heavily pigmented IPE provides only a background tint [IBK*96, IWA97]. It plays a minor role on iridal colour since it reflects only a small portion of the incident light, and its pigmentation does not present a detectable variance between irides of different colours [Eag88].

Two types of melanin are present in the human iris: the brown-black eumelanin and the red-yellow pheomelanin. The former is found in larger concentrations than the latter [MBP*87]. Experiments by Prota et al. [PHV*98] indicate that lightly pigmented irides show a low content of both pigments, while heavily pigmented irides exhibit a high content. Wistrand et al. [WSO97] also pointed out that irides with mixed hues usually have higher melanin concentration in the region around the pupil, known as the pupillary zone [SBM*94], and in the bottom of iridal depressions called crypts [SBM*94].

Besides the melanins, other natural pigments, notably the hemoglobins and the carotenoids, may contribute to the iridal spectral characteristics of healthy human eyes. The two types of hemoglobins (oxygenated and deoxygenated) are found in the stromal blood vessels [FDML02]. Similarly, two types of carotenoids (lutein and zeaxanthin) are also found in the Stromal Layer [BKC*01]. It has been suggested that a pigment called lipofuscin [TMA87] may also contribute to iridal chromatic variations [LCR*03]. However, to the best of our knowledge, quantitative evidence to fully

support this hypothesis for healthy human irides have not become available in the biomedical literature to date. Its occurrence in the human eye is usually associated with age-related degeneration of ocular fundus tissues [GWA99].

3. The ILIT Model

The proposed model has an algorithmic formulation in which light is represented by discrete rays, each one associated with a wavelength. Although geometrical optics is used in the light transport simulations performed by the model, wave optics approximations are employed where appropriate (*e.g.*, the computation of the optical free path length for a given ray traversing the iridal tissues at a given wavelength). The ILIT model simulates light interaction with human iris through a stochastic process whose states are represented by the interface between the iris and the surrounding medium, and the interfaces between adjacent iridal tissues, namely ABL, Stromal Layer and IPE. It is assumed that light transmitted to the IPE is absorbed within this tissue (Section 2.2).

A ray that traverses from one iridal layer to the next must pass the interface between these layers. At these interfaces the rays can be reflected or refracted. The results of these interactions are associated with the transition probabilities of the stochastic process, *i.e.*, they determine the next layer that the ray will traverse, thus its next state. Scattering events affecting the ray direction of propagation may also prompt the transition from one state to another. Absorption events are associated with the termination probabilities of the stochastic process, *i.e.*, when a ray is absorbed its transport simulation is halted.

Figure 3 illustrates possible paths that can be followed by a ray traversing the iridal tissues as well as the occurrence of scattering and absorption events. The non-deterministic simulation of these events employs random numbers u_i, for $i = 1, 2, \ldots 9$, uniformly distributed in the interval $[0, 1]$, which are generated on the fly during the simulations.

3.1. Reflection and Refraction at the Interfaces

Since each layer is simulated with its unique refractive index, either reflection or refraction occurs at all the interfaces. The ILIT model simulates these interactions by computing the Fresnel coefficient (F) associated with the incoming ray, and taking into account the refractive index differences of the media. If $u_1 \leq F$, then the ray is reflected. Otherwise, it is refracted. The Fresnel coefficients are computed through the Fresnel equations [Shi90].

3.2. Diffuse Perturbation

When a ray enters either the ABL or the Stromal Layer (Figure 4), it is diffusively perturbed due to the internal arrangement of the tissues (Section 2.2). In order to account for this effect, the ILIT model uses a warping function based on a

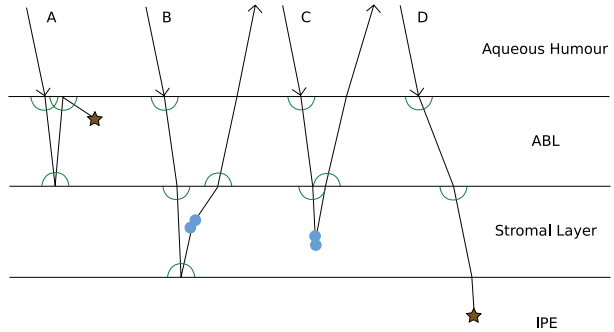

Figure 3: *Diagram illustrating possible paths (A, B, C and D) that can be followed by rays traversing the iridal tissues. The semi-circles represent diffuse perturbation, the double circles represent Rayleigh scattering (forward or backward), and the stars represent absorption events.*

cosine distribution [Shi90]. According to this function, the polar (α_d) and azimuthal (β_d) angles of the diffusively propagated rays, $\vec{v}_d$, are given by:

$$(\alpha_d, \beta_d) = (\arccos((1-u_2)^{\frac{1}{2}}), 2\pi u_3). \quad (1)$$

3.3. Absorption

When a ray is traversing either the ABL or the Stromal Layer, the ILIT model tests for its possible absorption (Figure 4) due to the presence of pigments (Section 2.2). As described by Prahl [Pra88], the probability of absorption of a photon (ray) traveling a distance Δp at a certain wavelength λ in a medium is given by :

$$P_{\mu_a}(\lambda) = 1 - \exp(-\mu_a(\lambda)\Delta p), \quad (2)$$

where $\mu_a(\lambda)$ represents the absorption coefficient of the medium. The absorption coefficient is obtained by adding the absorption coefficients of the medium's constituent materials, which, in turn, are computed by multiplying their spectral molar absorption (extinction) coefficient by their concentration in the medium.

In the case of the ABL, this probability is obtained using:

$$P_{\mu_{a_A}}(\lambda) = 1 - \exp\left(-\mu_{a_A}(\lambda)\frac{h_A}{\cos\theta}\right), \quad (3)$$

where $\mu_{a_A}(\lambda)$ represents the absorption coefficient of the ABL, which is computed using the concentrations of eumelanin and pheomelanin present in this tissue (Section 2.2), h_A represents to the thickness of the ABL, and $\theta < 90^\circ$ corresponds to the angle between the ray direction and the tissue's normal direction.

If $P_{\mu_{a_A}}(\lambda) \leq u_4$, then the ray is absorbed. Otherwise, the ray is propagated until it reaches the next interface.

In the Stromal Layer, the test for absorption is combined with the test for Rayleigh scattering, and these are described in more detail in the following section.

3.4. Attenuation

When a ray traverses the Stromal Layer, it may be attenuated (Figure 4). An attenuation event can be represented by either an absorption or a scattering event, and the attenuation coefficient, $\mu(\lambda)$, is simply the sum of the absorption and scattering coefficients. The former, in this case, corresponds to the absorption coefficient of the Stromal Layer, $\mu_{a_S}(\lambda)$, which is computed using the concentrations of melanins, hemoglobins and carotenoids present in this tissue (Section 2.2). The latter is derived in this section in terms of Rayleigh scattering caused by stromal collagen fibrils (Section 2.2).

It is assumed that the volume occupied by each collagen fibril of radius r can be approximated by a small sphere with the same radius [Jac96], which results in a scatterer density given by:

$$N = \left(\frac{4}{3}\, r^3\, \pi\right)^{-1} f_{collagen}, \tag{4}$$

where $f_{collagen}$ corresponds to the volume fraction of the tissue occupied by the scatterers (the collagen fibrils). Using this density, the scattering coefficient can be computed using the following expression [Str71]:

$$\mu_s(\lambda) = \frac{8\pi^3}{3N}((\eta(\lambda))^2 - 1)^2(\lambda^{-4}), \tag{5}$$

where η represents the refractive index of the scatterers.

Equation 5 was originally developed for the study of atmospheric scattering [Str71]. However, unlike atmospheric simulations where the scatterers are usually assumed to be dispersed in vacuum, our simulations need to account for the fact that the collagen fibrils, with their own refractive index $\eta_{collagen}$, are dispersed in iridal base material with a refractive index $\eta_{base} \neq 1.0$. Hence, in our simulations, η in Equation 5 is replaced by the ratio $\eta_{collagen}(\lambda)/\eta_{base}(\lambda)$.

After computing the absorption and scattering coefficients, the attenuation probability is obtained using:

$$P_\mu(\lambda) = 1 - \exp\left(-\mu(\lambda)\, \frac{h_S}{\cos\theta}\right), \tag{6}$$

where h_S represents the thickness of the Stromal Layer, and $\theta < 90^\circ$ corresponds to the angle between the ray direction and the tissue's normal direction.

If $u_5 > P_\mu(\lambda)$, then neither absorption nor scattering occurs. Otherwise, we need to determine the attenuation type. For this purpose, the absorption probability is computed as follows:

$$P_{\mu_{a_S}}(\lambda) = \frac{\mu_{a_S}(\lambda)}{\mu(\lambda)}. \tag{7}$$

If $u_6 \leq P_{\mu_{a_S}}(\lambda)$, then the ray is absorbed. Otherwise, the ray is scattered, and its new direction is determined according to the Rayleigh scattering phase function [vdH80], *i.e.*,

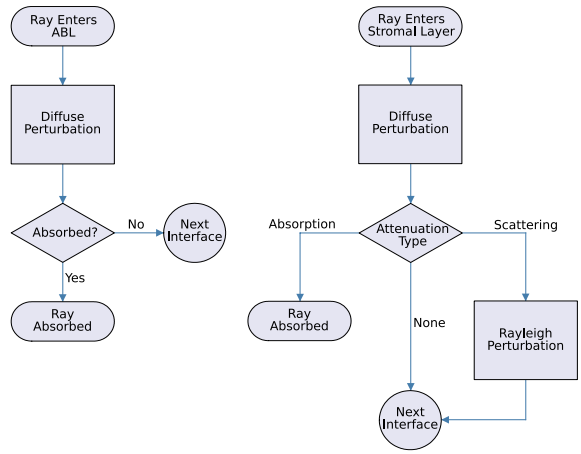

Figure 4: *Flowcharts illustrating the algorithms used by the ILIT model to simulate light transport in the ABL (left) and Stromal Layer (right).*

using rejection sampling, we repeatedly generate the polar perturbation angle:

$$\alpha_R = 2\pi u_7,$$

and accept it only when

$$u_8 \leq 0.5(1 + \cos^2\alpha_R).$$

Since the directional perturbation in the azimuthal direction is symmetric [vdH80], the azimuthal perturbation angle is simply given by $\beta_R = 2\pi u_9$. Hence, the new ray direction is obtained by perturbing it according to the angular displacements given by α_R and β_R.

4. Evaluation Procedures and Biophysical Data

In order to assess the accuracy and predictability of the proposed model, we compared modeled results with actual iridal data measured by Imai [Ima00] and Unander [Una00], as well as qualitative reports on the iridal spectral and spatial light distributions available in the scientific literature. For the latter, virtual measurement devices [Lam06] were implemented to allow the gathering of modeled reflectance and BRDF (bidirectional reflectance distribution function) data. For the former, the computational experiments took into account the actual measurement conditions to avoid the introduction of bias in the comparisons. For example, to obtain model readings in terms of the radiometric quantity measured by Imai [Ima00] and Unander [Una00], namely reflected radiance, the number of rays per wavelength shot towards the virtual iridal specimen was modulated according to the spectral characteristics of the light source used in the actual measurements [Lam06]. In addition, since the actual measurements were performed under *in vivo* conditions, the refractive indices of the tear layer, cornea and the aqueous humor, represented by $\eta_{tear}(\lambda)$, $\eta_{cornea}(\lambda)$ and $\eta_{ah}(\lambda)$ respectively, were used to determine the fraction of light incident on the virtual iridal specimen. We note, how-

ever, that no compensation was applied to account for a possible wavelength dependency of the cornea and aqueous humor transmittances [BW62]. This decision was made based on the observation that, to the best of our knowledge, the compensation formulas currently available in the literature [BvB90, vdBT94] were obtained by applying fitting approaches to data whose measurement did not account for backscattering [BW62]. Another simulation decision taken to match the actual experiment set up was the elimination of the rays directly reflected from the tear layer. We note that specular reflections were carefully excluded by Imai [Ima00] and Unander [Una00] in the actual measurements.

The quantitative values used for the model parameters were chosen according to data published in the biophysical literature. For certain parameters, however, data is not readily available, and it was necessary to derive approximated values from existing data. For example, to obtain the refractive indices for the ABL and the Stromal Layer, we applied the Gladstone and Dale's law [Tuc00], which states that the refractive index of a given material can be expressed by the sum of the refractive indices of its components, each weighted by the volume fraction occupied by the respective component. Accordingly, the following expression was used for the refractive index of the ABL:

$$\eta_A(\lambda) = \eta_{fibroblast}(\lambda)\ f_{fibroblast} + \eta_{base}(\lambda)\ (1 - f_{fibroblast}), \tag{8}$$

where $\eta_{fibroblast}(\lambda)$ and $f_{fibroblast}$ represent the refractive index and the volume fraction of the fibroblasts respectively. Similarly, the following expression was used for the refractive index of the Stromal Layer:

$$\eta_S(\lambda) = \eta_{collagen}(\lambda)\ f_{collagen} + \eta_{base}(\lambda)\ (1 - f_{collagen}). \tag{9}$$

For the IPE, based on its morphological characteristics (Section 2.2), a suitable approximation corresponds to the refractive index of the ocular base material [KMTW02]. This approximation was used in our simulations. Although refractive indices are wavelength dependent quantities, we remark that, for ocular materials, usually a single value over the visible range is available in the literature. The refractive indices used in the evaluation of the ILIT model are given in Table 1, and the values for $f_{fibroblast}$ and $f_{collagen}$ correspond to $1/3$ and $\pi/(4\sin(\pi/3))$ respectively. The former was provided by Snell and Lemp [SL89], and the later was obtained by considering stromal collagen fibrils with radius equal to $30nm$ [SL89] distributed in an hexagonal arrangement with a periodicity of $60nm$ [SL89].

Also due to the fact that the actual measurements were performed under *in vivo* conditions, we cannot determine the exact values for the thickness of the subjects' iridal layers. Hence, we used $h_A = 0.05675mm$ and $h_S = 0.2855mm$ in our simulations, which correspond to average values provided in the biomedical literature [Nol79, Eag88]. For the same reason, the values for the pigment concentrations, which are given below, were chosen according to average ranges reported for different pigmentation levels in the biomedical literature [BKC*01, Fle00, PHV*98], and considering a virtual iridal specimen with a diameter of $11mm$ [Nol79, Wil97] (which accounts for a pupillary radius of $2.5mm$ [Nol79]).

Table 1: *Refractive indices used in the simulations.*

Symbol	Value	Source
η_{tear}	1.337	[Duc90]
η_{cornea}	1.3771	[WS82]
η_{ah}	1.336	[EHR79]
$\eta_{fibroblast}$	1.42	[KMTW02]
η_{base}	1.5	[KMTW02]
$\eta_{collagen}$	1.47	[Tuc00]

The spectral properties of three different types of irides were considered in the actual measurements, namely lightly, moderately and heavily pigmented. The melanin concentration values used in the evaluation of the ILIT model are given in Table 2, and they were computed from data measured by Prota et al. [PHV*98] for different iridal types. The concentration values for the oxyhemoglobin and deoxyhemoglobin, $0.042mmol/l$ and $0.042mmol/l$ respectively, were obtained by assuming that the Stromal Layer contains approximately 4% of blood [Jac96], and taking into account that the concentration of hemoglobin in blood is typically $2.1mmol/l$ [Fle00]. The values selected for the lutein and zeaxanthin concentrations were $1.562 \times 10^{-4} mg/ml$ and $5.968 \times 10^{-5} mg/ml$ respectively, and they were computed from data provided by Bernstein et al. [BKC*01].

Table 2: *Melanin concentrations (mg/ml) used in the simulations.*

Pigment	Pigmentation Level		
	High	Moderate	Low
eumelanin	1.008	0.8138	0.1201
pheomelanin	0.2674	0.2054	0.0194

In our experiments, we used spectral molar absorptions curves for melanins and hemoglobins available at the Oregon Medical Laser Center [Lam06] and spectral molar absorptions curves for carotenoids provided by Zscheile et al. [ZWBR42]. We also account for the lengthening of the optical path of a tissue due to the inhomogeneous distribution of pigments under *in vivo* conditions [Fuk87]. This lengthening is called factor of intensification since it may result in an absorption increase when a pigment's concentration exceeds a certain threshold [Vog93]. Based on values reported in the tissue optics literature for natural pigments with similar concentrations [Vog93, Lam06], we apply a factor of intensification of 2.2 to the melanin absorption curves used in our experiments.

5. Results and Discussion

Quantitative comparisons of model readings with actual data measured by Imai [Ima00] and Unander [Una00] for three iridal specimens (lightly pigmented, moderately pigmented and heavily pigmented) are presented in Figure 5. These comparisons indicate a good quantitative and qualitative agreement between modeled and measured curves. The results provided by the ILIT model were obtained using the data provided in the previous section, and considering an equal distribution of melanin between the ABL and the Stromal Layer.

As mentioned in Section 2.2, biophysical parameters such as pigment concentration and tissue thickness are not uniform across the human iris. Hence, the measured spectral responses may vary depending on the measurement position. The variations observed in the experiments by Imai [Ima00] and Unander [Una00] are represented by error bars in the graphs presented in Figure 5. For the heavily pigmented specimen, the modeled curve is slightly outside the measured range. For the moderately and lightly pigmented specimens, the modeled curves are almost entirely within the variation range observed in the actual measurements.

Two aspects shall be taken into account in the analysis of these quantitative comparisons. First, we remark that the model input (characterization) data correspond to the best possible match that we could obtain between the specimens' description and data available in the literature, which, in several instances, correspond to average values. Hence, although the ILIT model can qualitatively simulate different spectral responses due to the variation of parameters such as pigment concentration and tissue thickness [Lam06], the quantitative accuracy of its predictions is limited by the availability of precise iridal characterization data, and the modeled curves presented in this paper can be viewed as average results themselves. Second, recall that biological data are usually obtained under *in vitro* conditions, and one may expect deviations from *in vivo* values. For example, the measurement of the extinction coefficient of a given pigment usually involves its dissolution using an organic solvent, and small spectral shifts caused by changes in the molecular properties of the pigments can be observed [Fuk87].

Besides the quantitative comparisons described above, we also performed qualitative comparisons against actual observations of real phenomena to assess the predictability of the ILIT model. As verified by Delori et al. [DDK91], the reflectance spectra of lightly pigmented irides present a characteristic blood signature ("w" shape) between 500*nm* to 600*nm* due to the characteristics of the absorption spectra of hemoglobin [Jac01], and this signature is not detectable in irides whose absorption spectra is dominated by melanins. The modeled reflectance curves presented in Figure 6 show that the ILIT model can account for this phenomenon. It can also be observed in the modeled reflected radiance curves (Figure 5) as the dip between 550*nm* to 600*nm* increases when the melanin concentration is reduced. Delori et al. [DDK91] also observed that iris reflectance among subjects with different levels of pigmentation varies most significantly at short wavelengths, reaching its maximum around 450*nm*. In addition, the range of this reflectance variation starts to decrease continuously around 600*nm*. These characteristics of iridal reflectance spectra can also be observed in the modeled reflectance curves presented in Figure 6. Incidentally, the premise that the iris becomes lighter (higher reflectance) as the melanin concentration decreases [WSF*96, WSO97] can also be verified in the modeled results shown in Figure 6.

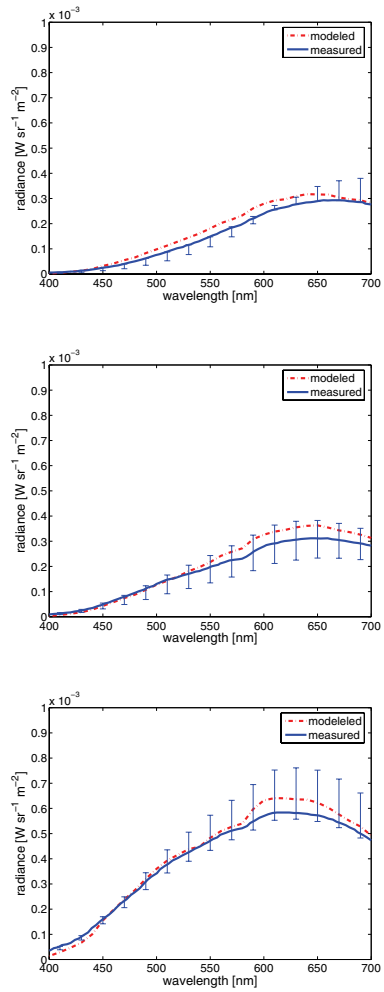

Figure 5: *Comparison of modeled reflected radiance curves provided by the ILIT model with actual reflected radiance curves measured by Imai [2000] and Unander [2000]. Top: heavily pigmented iris specimen. Center: moderately pigmented specimen. Bottom: lightly pigmented specimen. The error bars indicate maximum and minimum values observed in the actual measurements.*

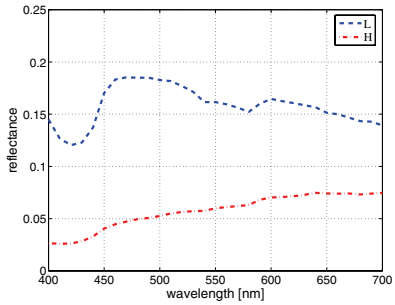

Figure 6: *Comparison of modeled reflectance curves provided by the ILIT model considering specimens with different levels of pigmentation: low (L) and high (H).*

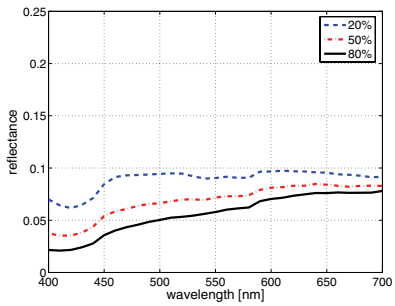

Figure 7: *Comparison of modeled reflectance curves provided by the ILIT model considering different melanin distributions between the ABL and the Stromal Layer (expressed in terms of the percentage of melanin presented in the ABL).*

According to observations by Menon et al. [MWP*92] and Imesh et al. [IBK*96], the distribution of the iridal melanin can also be a determinant of iridal chromatic attributes, with a more pigmented ABL resulting in a darker (lower reflectance) iris. We performed simulations to assess the predictability of the ILIT model with respect to this phenomenon. For these simulations we selected, without loss of generality, a moderately-pigmented iris specimen, and we varied the distribution of melanin between the ABL and the Stromal Layer. The modeled results shown in Figure 7 indicate that the ILIT model can qualitatively account for these chromatic variations.

Our qualitative experiments also included the verification of the iridal spatial light distributions provided by the ILIT model (expressed in terms of BRDFs). Although its role on the visual appearance of the human eye may be not as significant as the iridal spectral signature, its characteristics can provide additional evidence of the correctness of the simulation algorithms used by the ILIT model. Figure 8 presents plots of modeled BRDFs obtained for iridal specimens with different levels of pigmentation. As illustrated in these plots, the modeled BRDFs exhibit a near-Lambertian

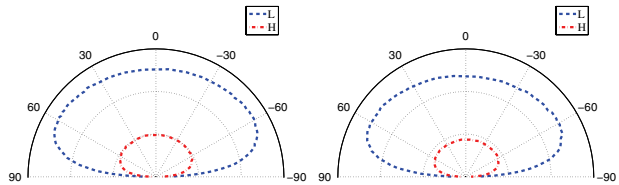

Figure 8: *Modeled iridal BRDFs measured at* 550*nm. Left: considering an angle of incidence of* 0°*. Right: considering an angle of incidence of* 60°*. Plots correspond to scattering profiles taken at the principal plane of incidence, and considering specimens with different levels of of pigmentation, namely low (L) and high (H).*

Figure 9: *Images showing iridal chromatic variations obtained using the ILIT model. From left to right, the iridal eumelanin concentration was decreased from* $1.008mg/ml$ *to* $0.1201mg/ml$*, and the iridal pheomelanin concentration from* $0.2674mg/ml$ *to* $0.0194mg/ml$*. From top to bottom, the percentage of melanin presented in the ABL was altered: 20% (top row), 50% (middle row) and 80% (bottom row).*

distribution which, as mentioned earlier (Section 2.2), corresponds to the general scattering profile of real human irides [BVM02, Wil97, WLLK05].

Finally, Figure 9 presents images rendered using the ILIT model (iris pattern and sclera taken from a photo), and taking as input the data provided in the previous section. These images illustrate chromatic variations obtained by changing the concentration and distribution of iridal melanins. We remark that the iridal chromatic attributes depicted in these images correspond solely to spectral signatures provided by the ILIT model, *i.e.*, to avoid the introduction of bias in our observations, post-processing tone adjustment techniques were not applied.

6. Conclusion and Future Work

The ILIT model is the first biophysically-based computer model proposed to simulate both the scattering and spectral properties of the human iris. Its evaluation showed a general

quantitative agreement between modeled results and actual measured data. It is important to note, however, that quantitative evaluations may be affected by inherent difficulties to characterize testing specimens. Hence, we believed that qualitative evaluations are also required to assess the predictability of a computer model. In the case of the ILIT model, the qualitative agreement between modeled results and observations of actual phenomena reported in the scientific literature represents an additional evidence of its predictive capabilities.

The algorithmic formulation of the ILIT model is based on standard Monte Carlo techniques which are sufficiently flexible to allow the modeling of complex phenomena within the iridal tissues. The stochastic simulations performed by the model, however, may be time consuming (in the order of hours) and represent a bottleneck in an image synthesis pipeline. Alternatively, these simulations could be either run off-line, and the quantities computed by the model stored and reconstructed on the fly during rendering, or performed using dedicated graphics hardware.

As future work, we intend to exploit the ILIT model on the assessment of theories and data relating iridal chromatic attributes to ocular medical conditions, and to extend our investigations to other ocular tissues and media. Although a reasonable amount of research on these materials is available in the biomedical literature, the computer graphics simulation of phenomena such as corneal polarization and tear film interference will require wave optics modeling tools to be brought to bear on the problem.

Acknowledgements

The authors would like to thank Dr. Francisco Imai for his valuable feedback on the procedures used on the actual iridal measurements, and the anonymous reviewers for their helpful suggestions. The work presented in this paper was supported by the Natural Sciences and Engineering Research Council of Canada (NSERC grant 238337) and the Canada Foundation for Innovation (CFI grant 33418).

References

[BASZ98] BERGAMIN O., A A. S., SUGIMOTO K., ZULAUF M.: The influence of iris color on the pupillary light reflex. *Graefes Arch. Clin. Exp. Ophthalmol. 236*, 8 (1998), 567–570.

[BKC*01] BERNSTEIN P., KHACHIK F., CARVALHO L., MUIR G., ZHAO D., KATZ N.: Identification and quantitation of carotenoids and their metabolites in the tissues of the human eye. *Experimental Eye Research 72* (2001), 215–223.

[BvB90] BEEMS E., VAN BEST J.: Light transmission of the cornea in the whole human eyes. *Experimental Eye Research 50* (1990), 393–395.

[BVM02] BUENO J., VARGAS-MARTIN F.: Measurements of the corneal birefringence with a liquid-crystal imaging polariscope. *Applied Optics 41*, 1 (2002), 116–124.

[BW62] BOETTNER E. A., WOLTER J. R.: Transmission of the ocular media. *Investigative Ophthalmology and Visual Science 1*, 6 (1962), 776–783.

[DD01] DAUGMAN J., DOWING C.: Epigenetic randomness, complexity and singularity of human iris patterns. *Proc. R. Soc. Lond. B 268* (2001), 1737–1740.

[DDK91] DELORI F., DOREY C., K.A.FITCH: Characterization of ocular melanin by iris reflectometry. *Investigative Ophthalmology and Visual Science 32*, 1-4 (1991), 1144.

[Dee05] DEERING M.: A photon accurate model of the eye. *ACM Transactions on Graphics 24*, 3 (2005), 649–658.

[DP89] DELORI F., PFLIBSEN K.: Spectral reflectance of the human ocular fundus. *Applied Optics 28*, 6 (1989), 1061–1077.

[Duc90] DUCK F.: *Physical Properties of Tissue: A Comprehensive Reference Book*. Academic Press Inc., California, U.S.A., 1990.

[Eag88] EAGLE R.: Iris pigmentation and pigmented lesions: An ultrastructural study. *Trans. Am. Ophth. Soc. 86* (1988), 581–687.

[EHR79] EDELHAUSER H., HORN D., RECORDS R.: Cornea and sclera. In *Physiology of the Human Eye and Visual System* (Maryland, U.S.A., 1979), Records R., (Ed.), Harper and Row Publishers Inc., pp. 68–97.

[FDML02] FORRESTER J., DICK A., MCMENAMIN P., LEE W.: *The Eye: Basic Sciences in Practice*, second ed. WB Saunders, Sydney, 2002.

[Fle00] FLEWELLING R.: Noninvasive optical monitoring. In *The Biomedical Engineering Handbook* (Boca Raton, FL, USA, 2000), Bronzino J., (Ed.), IEEE Press, pp. 1–11. Section 86.

[Fuk87] FUKSHANSKY L.: Absorption statistics in turbid media. *Journal of Quantitative Spectroscopy and Radiative Transfer 38*, 5 (1987), 389–406.

[GWA99] GENG L., WIHLMARK U., ALGVERE P. V.: Lipofuscin accumulation in iris pigment epithelial cells exposed to photoreceptor outer segments. *Experimental Eye Research 69* (1999), 539–546.

[HBKM96] HALSTEAD M., BARSKY B., KLEIN S., MANDELL R.: Reconstructuring curved surfaces from specular reflection patterms using spline surface fitting of normals. In *SIGGRAPH, Annual Conference Series* (1996), pp. 335–342.

[HRSM95] HAMMER M., ROGGANT A., SCHWEITZER D., MULLER G.: Optical properties of ocular fundus tissues - and in vitro study using the double-integrating-sphere technique and inverse Monte Carlo simulation. *Physics in Medicine and Biology 40* (1995), 963–978.

[HS02] HAMMER M., SCHWEITZER D.: Quantitative reflection spectroscopy at the human ocular fundus. *Physics in Medicine and Biology 47* (2002), 179–191.

[IBK*96] IMESCH P., BINDLEY C., KHADEMIAN Z., LADD B., GANGNON R., ALBERT D., WALLOW I.: Melanocytes and iris color, electron microscopic findings. *Archives of Ophthalmology 114* (1996), 443–447.

[Ima00] IMAI F.: *Preliminary Experiment for Spectral Reflectance Estimation of Human Iris using a Digital Camera*. Tech. rep., Munsell Color Science Laboratory, Rochester Institute of Technology, Rochester, N.Y., U.S.A., 2000.

[IWA97] IMESCH P., WALLOW I., ALBERT D.: The color of the human eye: A review of morphologic correlates and of some conditions that affect iridial pigmentation. *Survey of Ophthalmology 41*, suppliment 2 (1997), S117–S123.

[Jac96] JACQUES S.: Origins of tissue optical properties in the uva visible and nir regions. *OSA TOPS on Advances in Optical Imaging and Photon Migration 2* (1996), 364–369.

[Jac01] JACQUES S.: *Optical Absorption of Melanin*. Tech. rep., Oregon Medical Laser Center, Portland, U.S.A, 2001.

[KMTW02] KHLEBTSOV N., MAKSIMOVA I., TUCHIN V., WANG L.: Introduction to light scattering by biological objects. In *Handbook of Optical Biomedical Diagnostics* (Bellingham, U.S.A., 2002), Tuchin V., (Ed.), SPIE Press, pp. 31–167.

[Lam06] LAM M.: *ILIT: A Predictive Light Transport Model for the Human Iris*. Master's thesis, School of Computer Science, University of Waterloo, Canada, 2006.

[LCR*03] LEFOHN A., CARUSO R., REINHARD E., BUDGE B., SHIRLEY P.: An ocularist's approach to human iris synthesis. *IEEE Computer Graphics and Applications 23*, 6 (2003), 70–75.

[MBP*87] MENON I., BASU P., PERSAD S., AVARIA M., FELIX C., KALYANARAMAN B.: Is there any difference in the photobiological properties of melanins isolated from human blue and brown eyes? *British Journal of Ophthalmology 71* (1987), 549–552.

[MWP*92] MENON I., WAKEHAM D., PERSAD S., AVARIA M., TROPE G. E., BASU P.: Quantitative determination of the melanin contents in ocular tissues from human blue and brown eyes. *Journal of Ocular Pharmacology 8*, 1 (1992), 35–42.

[Nol79] NOLTE J.: Iris and pupil. In *Physiology of the Human Eye and Visual System* (Maryland, U.S.A., 1979), Records R., (Ed.), Harper and Row Publishers Inc., pp. 217–231.

[PC02] PREECE S., CLARIDGE E.: Monte Carlo modelling of the spectral reflectance of the human eye. *Physics in Medicine and Biology 47* (2002), 2863–2877.

[PHV*98] PROTA G., HU D., VINCENSI M. R., MCCORMICK S., NAPOLITANO A.: Characterization of melanins in human irides and cultured uveal melanocytes from eyes of different colors. *Experimental Eye Research 67* (1998), 293–299.

[Pra88] PRAHL S.: *Light Transport in Tissue*. PhD thesis, The University of Texas at Austin, TX, USA, December 1988.

[Pur03] PURGATHOFER W.: Open issues in photo-realistic rendering. *Computer Graphics Forum 22*, 3 (2003), xix.

[REG97] REGAN S., EGAN K., GRAGOUDAS E.: Iris color as a risk factor in uveal melanoma. *Investigative Ophthalmology and Visual Science 38*, 4 (1997), S810.

[SBM*94] SAGAR M., BULLIVANT D., MALLINSON G., HUNTER P., HUNTER I.: A virtual environment and model of the eye for surgical simulation. *SIGGRAPH, Annual Conference Series* (1994), 205–213.

[Shi90] SHIRLEY P.: *Physically Based Lighting for Computer Graphics*. PhD thesis, Dept. of Computer Science, University of Illinois, November 1990.

[SL89] SNELL R., LEMP M.: *Clinical Anatomy of The Eye*. Blackwell Scientific Publications, Massachusetts, U.S.A., 1989.

[Str71] STRUTT J.: On the scattering of light by small particles. *Philosophical Magazine 41*, 275 (June 1871), 447–454.

[TMA87] TSUCHIDA M., MIURA T., AIBARA K.: Lipofuscin and lipofuscin-like substances. *Chemistry and Physics of Lipids 44* (1987), 297–325.

[TSC*01] TAKAMOTO T., SCHWARTZ B., CANTOR L. B., HOOP J. S., STEFFENS T.: Measurement of iris color using computerized image analysis. *Current Eye Research 22*, 6 (2001), 412–419.

[Tuc00] TUCHIN V.: *Tissue Optics: Light Scattering Methods and Instruments for Medical Diagnosis, Tutorial Texts in Optical Engineering Volume TT38*. SPIE - The International Society for Optical Engineering, Washington, U.S.A., 2000.

[Una00] UNANDER J.: *Project Iris: Image Reconstruction of the Iris Spectrally*. Tech. rep., Munsell Color Science Laboratory, Rochester Institute of Technology, Rochester, U.S.A., 2000.

[vdBT94] VAN DEN BERG T., TAN K.: Light transmittance of the human cornea from 320 to 700nm for different ages. *Vision Research 34*, 11 (1994), 1453–1456.

[vdH80] VAN DE HULST H.: *Multiple Light Scattering: Tables, Formulas, and Applications*, vol. 1. Academic Press, New York, U.S.A., 1980.

[vNT86] VAN NORREN D., TIEMEIJER L.: Spectral reflectance of the human eye. *Vision Research 26*, 2 (1986), 313–320.

[Vog93] VOGELMANN T.: Plant tissue optics. *Annual Review of Plant Physiology and Plant Molecular Biology 44* (1993), 231–251.

[WFG05] WECKER L., F.SAMAVATI, GAVRILOVA M.: Iris synthesis: A reverse subdivision technique. In *3rd International Conference on Computer Graphics and Interactive Techniques in Australasia and South East Asia* (Dunedin, New Zealand, November 2005), pp. 121–125.

[WG70] WYATT H., GHOSH J.: Behaviour of an iris model and the pupil block hypothesis. *British Journal of Ophthalmology 54* (1970), 177–185.

[Wil97] WILDES R.: Iris recognition: An emerging biometric technology. *Proceedings of IEEE 85*, 9 (1997), 1348–1363.

[WLLK05] WANG H., LIN S., LIU X., KANG S.: Separating reflections in human iris images for illumination estimation. In *ICCV* (2005), pp. 1691–1698.

[WS82] WYSZECKI G., STILES W.: *Color Science, Concepts and Methods, Quantitative Data and Formulae*, 2nd ed. John Wiley and Sons, Inc., New York, U.S.A., 1982.

[WSF*96] WILKERSON C., SYED N., FISHER M., ROBINSON N., WALLOW I., ALBERT D.: Melanocytes and iris color, light microscopic findings. *Archives of Ophthalmology 114* (1996), 437–442.

[WSO97] WISTRAND P., STJERNSCHANTZ J., OLSSON K.: The incidence and time-course of latanoprost-induced iridial pigmentation as a function of eye color. *Survey of Ophthalmology 41* (1997), S129–S138.

[ZWBR42] ZSCHEILE F., WHITE J., BEADLE B., ROACH J.: The preparation and absorption spectra of five pure carotenoid pigments. *Plant Physiology 17*, 3 (1942), 331–346.